A Three-Dimensional Variational Data Assimilation Scheme in Support of Coastal Ocean Observing Systems

Zhijin Li[a], Yi Chao[a],John D. Farrara[b], Xiaochun Wang[b], James C. McWilliams[c], and Kayo Ide[c]

[a] Jet Propulsion Laboratory, California Institute of Technology, Pasadena, USA;
[b] Raytheon Intelligence and Information Systems, Pasadena, USA;
[c] University of California, Los Angeles, USA

ABSTRACT

A three-dimensional variational data assimilation (3DVAR) system (ROMS3DAR) has been developed in the framework of the Regional Ocean Modeling System (ROMS). This system enables the capability of predicting meso- to small-scale variations with temporal scales from hours to days in the coastal oceans. To cope with the particular difficulties that result from complex coastlines and bottom topography, unbalanced flows and sparse observations, ROMS3DVAR utilizes several novel strategies. These strategies include the implementation of three-dimensional anisotropic and inhomogeneous error correlations, application of particular weak dynamic constraints, and implementation of efficient and reliable algorithms for minimizing the cost function. ROMS3DVAR has been implemented in a quasi-real-time fashion in support of both the Southern and Central California Coastal Ocean Observing System (SCCOOS and CenCOOS). ROMS3DVAR assimilates a variety of observations, including satellite sea surface temperatures and sea surface heights, High Frequency (HF) radar velocities, ship reports and other available temperature and salinity profiles. The evaluation showed useful forecast skills.

Keywords: data assimilation, coastal ocean, observing system, satellite data, glider, High Frequency radar

1. INTRODUCTION

There are multiple ongoing efforts in the federal and state government to establish a network of coastal ocean observing systems that will suit both research and operational needs. As a consequence, we have been seeing an explosive development of new observational tools and platforms. Development in satellite oceanography provides unprecedented views of the ocean with increasing resolutions and accuracy, coupled with capabilities of measuring new variables (e.g., sea surface salinity). We also envision a new generation of *in situ* observations, ranging from autonomous instruments and probes to cabled observatories. Shore-based High-Frequency (HF) radars provides spatially and temporally continuous sea surface velocity maps. Coastal oceanography is in a rapid transition from an era of exploratory mapping and sampling to one of real-time observing systems.

Real-time observing systems will make it possible to develop predictive numerical modeling systems that will routinely provide coastal oceanic "weather" predictions as today's meteorological models routinely provide numerical weather predictions for the atmosphere. A predictive modeling system requires two basic components: an advanced numerical model and real-time data assimilation system.[1] In this paper we present a three-dimensional variational data assimilation (3DVAR) algorithm within the framework of the Regional Ocean Modeling System (ROMS)[2].[3] This system is called ROMS3DVAR.

ROMS3DVAR was developed as an operational data assimilation system similar to those implemented in major meteorological centers and thus possesses the following capabilities. First, it generates initial conditions that ROMS uses to predict future coastal oceanic states; second, it provides basic analyzed fields for various users, including oceanic forecasters and the public; and, third, it produces data sets for various diagnostic analyses, such as those used for health monitoring. ROMS3DVAR also has the capability to being used as a numerical testbed

Further author information: (Send correspondence to Zhijin Li)
Zhijin Li: E-mail: zhijin.li@jpl.nasa.gov, Telephone: 1 818 393 9058

for the evaluation and assessment of new types of measurements. ROMS3DVAR was developed to maximize flexibility and stability in assimilating different types of new measurements. For example, it allows simultaneous assimilation of measurements ranging from radial velocities from High Frequency (HF) radars[4] to radiances from satellite-flown remote sensing instruments. Moreover, assimilation of chemical and biological quantities can be formulated as an extension of the physical quantities. For example, biological concentrations can be treated in the same way as salinity. We here present the formulation of ROMS3DAR and its performance as implemented in the coastal regions off Central California (http://ourocean.jpl.nasa.gov/MB06) as an operational system.

This paper is organized as follows: Section 2 presents the basic formulation of ROMS3DVAR. Section 3 details the particular formulation of the dynamic constraints. Section 4 is dedicated to estimation and modeling of error covariance, especially the Kronecker product-based algorithms proposed to model error correlations. In section 6, the evaluation of 24h forecast are presented. Section 7 gives a summary.

2. THREE-DIMENSIONAL VARIATIONAL DATA ASSIMILATION

In this section, we will describe the basic formulation of ROMS3DVAR as a three-dimensional variational data assimilation system. We will follow the notation conventions suggested by Ide et al.[5] Vectors will be represented by boldface lowercase letters, and matrices by boldface uppercase letters and Greek letters. Also, the superscript "f" stands for forecast, the superscript "a" for analysis, the superscript "t" for truth, the superscript "T" for matrix transpose, and the symbol $< \cdot >$ for mathematical expectation.

The formulation presented in this paper will involve only the physical components of ROMS for simplicity, though ROMS has chemical, biological and other components. The physical variables in ROMS are sea surface height (SSH) ζ, horizontal velocity components u and v, temperature T, and salinity S.

The model state can be written as a vector, consisting of the values of ζ, u, v, T and S at the model grid points. We use $\mathbf{x}_u$, $\mathbf{x}_v$, $\mathbf{x}_T$, $\mathbf{x}_S$, and $\mathbf{x}_\zeta$ for the model state along with N_u, N_v, N_T, N_S, and N_ζ for their dimensions as denoted by the corresponding subscript. For convenience, we organize them into three groups, $\mathbf{x}_\zeta$, $\mathbf{x}_{uv} = (\mathbf{x}_u^T, \mathbf{x}_v^T)^T$ for velocity with dimension $N_{uv} = N_u + N_v$, $\mathbf{x}_{TS} = (\mathbf{x}_T^T, \mathbf{x}_S^T)^T$ for T and S with dimension $N_{TS} = N_T + N_S$. Altogether, the net state vector $\mathbf{x}$ of ROMS at a given time can be written as

$$\mathbf{x} = \begin{pmatrix} \mathbf{x}_\zeta \\ \mathbf{x}_{uv} \\ \mathbf{x}_{TS} \end{pmatrix}, \tag{1}$$

where $N = N_\zeta + N_u + N_v + N_T + N_S$ is dimension of $\mathbf{x}$.

In data assimilation, the model state is combined with observations. Generally the M-dimensional observation vector $\mathbf{y}$ is related to the model state $\mathbf{x}$ by

$$\mathbf{y} = \boldsymbol{\mathcal{H}}(\mathbf{x}^{\mathrm{t}}) + \mathbf{e}, \tag{2}$$

where $\mathbf{x}^{\mathrm{t}}$ is the unknown true state to be estimated; $\boldsymbol{\mathcal{H}}$ is the observational operator that maps the model state to the observation location, and $\mathbf{e}$s is the observational error.

We consider that three types of observations are available: M_ζ-dimensional SSH observation $\mathbf{y}_\zeta$, M_{uv}-dimensional velocity observation $\mathbf{y}_{uv}$, and M_{TS}-dimensional T and S observation $\mathbf{y}_{TS}$. Similar to a model state, we write the net observation as

$$\mathbf{y} = \begin{pmatrix} \mathbf{y}_\zeta \\ \mathbf{y}_{uv} \\ \mathbf{y}_{TS} \end{pmatrix}, \tag{3}$$

where $M_{obs} = M_\zeta + M_{uv} + M_{TS}$ is the total number of observations. When the observational operator is linear, we have $\boldsymbol{\mathcal{H}}(\mathbf{x}) = \mathbf{H}\mathbf{x}$, where

$$\mathbf{H} = \begin{pmatrix} \mathbf{H}_\zeta & \mathbf{0}_{M_\zeta \times N_{uv}} & \mathbf{0}_{M_\zeta \times N_{TS}} \\ \mathbf{0}_{M_{uv} \times N_\zeta} & \mathbf{H}_{uv} & \mathbf{0}_{M_{uv} \times N_{TS}} \\ \mathbf{0}_{M_{TS} \times N_\zeta} & \mathbf{0}_{M_{TS} \times N_{uv}} & \mathbf{H}_{TS} \end{pmatrix}. \tag{4}$$

is the $M \times N$-dimensional observation matrix; $\mathbf{H}_\zeta$ is the $M_\zeta \times N_\zeta$-dimensional SSH observation matrix; $\mathbf{H}_{uv}$ is $M_{uv} \times N_{uv}$-dimensional velocity observation matrix; $\mathbf{H}_{TS}$ is $M_{TS} \times N_{TS}$-dimensional velocity observation matrix; and $\mathbf{0}_{M_* \times N_*}$ stands for the $M_* \times N_*$-dimensional zero matrix. When a type of observation is unavailable, corresponding rows are removed from $\mathbf{y}$ and $\mathbf{H}$ in (2) and (4). For simplicity in presentation, the dimension of vectors and matrices is noted only when necessary from here on.

The incremental formulation has been used as a basic approximation in operational 3DVAR systems.[6] When a forecast is accurate, the analysis increment is a small derivation from the forecast. This grants a foundation for linearization around $\mathbf{x}^f$ in $J(\mathbf{x})$. It is a reasonable assumption for current coastal ocean models like ROMS. In the incremental 3DVAR formulation, the cost function is defined by

$$J_{inc}(\delta\mathbf{x}) = \frac{1}{2}\delta\mathbf{x}^T\mathbf{B}^{-1}\delta\mathbf{x} + \frac{1}{2}(\mathbf{H}\delta\mathbf{x} - \mathbf{d})^T\mathbf{R}^{-1}(\mathbf{H}\delta\mathbf{x} - \mathbf{d}). \tag{5}$$

The first and second terms are often referred to as the background and observational cost functions. Here $\delta\mathbf{x} = \mathbf{x} - \mathbf{x}^{\mathrm{f}}$ is the increment, measuring the deviation of $\mathbf{x}$ from $\mathbf{x}^{\mathrm{f}}$; $\mathbf{d} = \mathbf{y} - \boldsymbol{\mathcal{H}}(\mathbf{x}^{\mathrm{f}})$ is the innovation, measuring the deviation of $\mathbf{y}$ from $\mathbf{x}^{\mathrm{f}}$; and $\mathbf{H} = \partial\boldsymbol{\mathcal{H}}/\partial\mathbf{x}$ is Jacobian matrix for nonlinear $\boldsymbol{\mathcal{H}}$. The incremental approximation makes $J_{inc}(\delta\mathbf{x})$ quadratic and positive definite in the control variable $\delta\mathbf{x}$. The quadratic and positive definite properties guarantee that $J_{inc}(\delta\mathbf{x})$ has a unique minimum, and this uniqueness is also essential for efficiency and reliability of the minimization process. The final analysis of the incremental 3DVAR is

$$\mathbf{x}^{\mathrm{a}} = \mathbf{x}^{\mathrm{f}} + \delta\mathbf{x}^{\mathrm{a}}, \tag{6}$$

where the analysis increment $\delta\mathbf{x}^{\mathrm{a}}$ minimizes $J_{inc}(\delta\mathbf{x})$.

3. DYNAMICAL CONSTRAINTS

ROMS3DVAR is designed to assimilate different types of observations simultaneously and reliably. Different types of observations come with different errors and generally are dynamically inconsistent. One challenge is to keep the obtained analysis in reasonable dynamic balance after the different types of observations are assimilated. For example, in many cases the velocity is nearly in geostrophic balance, but the data assimilation algorithm described above has no capability for keeping the velocity analysis close in geostrophic balance.

In ROMS3DVAR we are concerned with two dynamic constraints. One is hydrostatic balance

$$\frac{\partial\delta p}{\partial z} = -g\delta\rho, \tag{7}$$

and the other is geostrophic balance

$$\vec{\Omega} \times \delta\vec{v} = -\rho^{-1}\nabla\delta p, \tag{8}$$

where both are written in the continuous form using pressure p, density ρ, gravitational acceleration g, angular velocity of Earth rotation $\vec{\Omega}$, and horizontal velocity vector $\vec{v}$. In the incremental form, (7) and (8) can be written as

$$\delta\zeta = -\frac{1}{\rho_0 + \rho_s^{\mathrm{f}}}\int_{-h_b}^{\zeta^{\mathrm{f}}} \delta\rho dz + \frac{\delta p_{h_b}}{\rho_0 + \rho_s^{\mathrm{f}}}. \tag{9}$$

$$-f\delta v = -\frac{g}{\rho_0 + \rho^{\mathrm{f}}}\frac{\partial}{\partial x}\int_{-h}^{\zeta^{\mathrm{f}}} \delta\rho dz - \frac{g(\rho_0 + \rho_s^{\mathrm{f}})}{\rho_0 + \rho^{\mathrm{f}}}\frac{\partial\delta\zeta}{\partial x}, \tag{10}$$

$$f\delta u = -\frac{g}{\rho_0 + \rho^{\mathrm{f}}}\frac{\partial}{\partial y}\int_{-h}^{\zeta^{\mathrm{f}}} \delta\rho dz - \frac{g(\rho_0 + \rho_s^{\mathrm{f}})}{\rho_0 + \rho^{\mathrm{f}}}\frac{\partial\delta\zeta}{\partial y}. \tag{11}$$

Here ρ_0 is the Boussinesque approximation of the mean density,ρ_s^{f} the forecast surface density increment, h_b the depth of the bottom, and p_{h_b} the bottom pressure. In the discrete form, we can know that hydrostatic balance relates $\delta\mathbf{x}_{TS}$ to $\delta\mathbf{x}_\zeta$, while geostrophic balance relates $\delta\mathbf{x}_{TS}$ and $\delta\mathbf{x}_\zeta$ to $\delta\mathbf{x}_{uv}$ These balance constraints can be

replaced by more sophisticated balance equations (e.g., McWilliams et al.[7]) in ROMS3DVAR, if necessary. Note that the balance constraints are applied to the increment, rather than the total field.

As known, $\delta\mathbf{x}_\zeta$ and $\delta\mathbf{x}_{uv}$ in the coastal ocean may not necessarily be in exact dynamic balance. Rather, they have both balanced and unbalanced components.[8] To formulate an incremental 3DVAR algorithm that has the capacity to address balanced and unbalanced components simultaneously, we follow the method proposed by Parrish and Derber.[9] Their method partitions the model state vector into slow (balanced) and fast (unbalanced) components. The control variables become the unbalanced components. Doing so imposes dynamic balance only partially and hence implements what are called weak constraints. This method has recently been applied in several different data assimilation systems[10].[11]

Based on the hydrostatic balance (7), $\delta\mathbf{x}_\zeta$ can be approximately represented in discrete form as

$$\delta\mathbf{x}_\zeta = \mathbf{\Pi}\delta\mathbf{x}_{TS} + \delta\mathbf{x}_{\zeta'} \tag{12}$$

where $\mathbf{\Pi}\delta\mathbf{x}_{TS}$ is the steric SSH that is in balance with the T and S increment (8), and $\delta\mathbf{x}_{\zeta'}$ is the non-steric SSH increment due to water mass convergence in the column. In contrast to ocean data assimilation with large scale models, $\delta\mathbf{x}_{\zeta'}$ is non-negligible for coastal data assimilation as illustrated in Li et al.[8]

Based on the geostrophic balance (8), $\delta\mathbf{x}_{uv}$ can be approximately represented in discrete form as

$$\delta\mathbf{x}_{uv} = \mathbf{\Gamma}_{TS}\delta\mathbf{x}_{TS} + \mathbf{\Gamma}_{\zeta'}\delta\mathbf{x}_{\zeta'} + \delta\mathbf{x}_{u''v''}, \tag{13}$$

where $\mathbf{\Gamma}_{TS}\delta\mathbf{x}_{TS} + \mathbf{\Gamma}_{\zeta'}\delta\mathbf{x}_{\zeta'}$ is the geostrophic velocity that is in balance with the pressure gradient (8) in a response to changes in steric and non-steric SSH (12), and $\delta\mathbf{x}_{u''v''}$ is the ageostrophic velocity. While $\mathbf{\Gamma}_{TS}\delta\mathbf{x}_{TS}$ due to T/S profile changes may be dominant offshore, $\mathbf{\Gamma}_{\zeta'}\delta\mathbf{x}_{\zeta'}$ due to non-steric SSH and ageostrophic $\delta\mathbf{x}_{u''v''}$ can be sizable nearshore.

In data assimilation, the streamfunction and velocity potential are more suitable than the velocity components for use as control variables in data assimilation.[12] As such, the incremental ageostrophic velocity $(\delta u'', \delta v'')$ may be written using the incremental ageostrophic streamfunction $\delta\psi''$ and the velocity potential $\delta\chi''$ as

$$\begin{aligned} \delta u'' &= -\frac{\partial\delta\psi''}{\partial y} + \frac{\partial\delta\chi''}{\partial x} \\ \delta v'' &= \frac{\partial\delta\psi''}{\partial x} + \frac{\partial\delta\chi''}{\partial y} \ . \end{aligned} \tag{14}$$

Using the discrete form of (14), (13) becomes

$$\delta\mathbf{x}_{uv} = \mathbf{\Gamma}_{\zeta'}\delta\mathbf{x}_{\zeta'} + \mathbf{\Gamma}_{TS}\delta\mathbf{x}_{TS} + \mathbf{\Phi}\delta\mathbf{x}_{\psi''\chi''}, \tag{15}$$

where $\delta\mathbf{x}_{\psi''\chi''}$ is the $N_{\psi\chi}$-dimensional vector, encompassing the discrete $\delta\psi''$ and $\delta\chi''$, and $\mathbf{\Phi}$ is a matrix for computing the velocity component from the streamfunction and velocity potential. A numerical method for computing streamfunction and velocity potential from the velocity components for irregular domains like coastal oceans is available.[13]

To adjust $J_{inc}(\delta\mathbf{x})$ for dynamic constraints, we assume that errors in $\delta\mathbf{x}_{\zeta'}$, $\delta\mathbf{x}_{\psi''\chi''}$ and $\delta\mathbf{x}_{TS}$ are uncorrelated to each other in the present ROMS3DVAR. A natural form of the control variable under the constraints chosen is then

$$\delta\mathbf{x}_c = \begin{pmatrix} \delta\mathbf{x}_{\zeta'} \\ \delta\mathbf{x}_{\psi''\chi''} \\ \delta\mathbf{x}_{TS} \end{pmatrix}, \tag{16}$$

whose linear relation to $\delta\mathbf{x}$ is given by (12) and (15). We further assume that observational errors $\mathbf{e}_\zeta$, $\mathbf{e}_{uv}$ and $\mathbf{e}_{TS}$ in $\mathbf{y}_\zeta$, $\mathbf{y}_{uv}$ and $\mathbf{y}_{TS}$ are also uncorrelated to each other as well as any errors in $\delta\mathbf{x}_c$. Accordingly, an incremental 3DVAR (5) can be formulated as the weak constraints:

$$\begin{aligned} J_c(\delta\mathbf{x}_c) &= J^{\mathrm{b}}_{\zeta'}(\delta\mathbf{x}_{\zeta'}) + J^{\mathrm{b}}_{\psi''\chi''}(\delta\mathbf{x}_{\psi''\chi''}) + J^{\mathrm{b}}_{TS}(\delta\mathbf{x}_{TS}) \\ &+ J^{\mathrm{o}}_{\zeta}(\delta\mathbf{x}_{\zeta'}, \delta\mathbf{x}_{TS}) + J^{\mathrm{o}}_{uv}(\delta\mathbf{x}_{\zeta'}, \delta\mathbf{x}_{\psi''\chi''}, \delta\mathbf{x}_{TS}) + J^{\mathrm{o}}_{TS}(\delta\mathbf{x}_{TS}) \ . \end{aligned} \tag{17}$$

The background cost function breaks up into three parts:

$$\begin{aligned} J^{\mathrm{b}}_{a\zeta} &= \frac{1}{2}\delta\mathbf{x}^T_{a\zeta}\mathbf{B}^{-1}_{a\zeta}\delta\mathbf{x}_{a\zeta} \\ J^{\mathrm{b}}_{\psi''\chi''} &= \frac{1}{2}\delta\mathbf{x}^T_{\psi''\chi''}\mathbf{B}^{-1}_{\psi''\chi''}\delta\mathbf{x}_{\psi''\chi''} \\ J^{\mathrm{b}}_{TS} &= \frac{1}{2}\delta\mathbf{x}^T_{TS}\mathbf{B}^{-1}_{TS}\delta\mathbf{x}_{TS}, \end{aligned} \tag{18}$$

where $\mathbf{B}_{\zeta'}$, $\mathbf{B}_{\psi''\chi''}$, and $\mathbf{B}_{TS}$ are the background error covariances corresponding to non-steric SSH; ageostrophic streamfunction and velocity potential; and T and S. The observational cost function also breaks up into three parts:

$$\begin{aligned} J^{\mathrm{o}}_{\zeta'} &= \frac{1}{2}(\mathbf{\Pi}\delta\mathbf{x}_{TS} + \delta\mathbf{x}_{\zeta'} - \mathbf{d}_{\zeta})^T\mathbf{R}^{-1}_{\zeta}(\mathbf{\Pi}\delta\mathbf{x}_{TS} + \delta\mathbf{x}_{\zeta'} - \mathbf{d}_{\zeta}) \\ J^{\mathrm{o}}_{uv} &= \frac{1}{2}(\mathbf{\Gamma}_{\zeta'}\delta\mathbf{x}_{\zeta'} + \mathbf{\Gamma}_{TS}\delta\mathbf{x}_{TS} + \mathbf{\Phi}\delta\mathbf{x}_{\psi''\chi''} - \mathbf{d}_{uv})^T\mathbf{R}^{-1}_{uv}(\mathbf{\Gamma}_{\zeta'}\delta\mathbf{x}_{\zeta'} + \mathbf{\Gamma}_{TS}\delta\mathbf{x}_{TS} + \mathbf{\Phi}\delta\mathbf{x}_{\psi''\chi''} - \mathbf{d}_{uv}) \\ J^{\mathrm{o}}_{TS} &= \frac{1}{2}(\delta\mathbf{x}_{TS} - \mathbf{d}_{TS})^T\mathbf{R}^{-1}_{TS}(\delta\mathbf{x}_{TS} - \mathbf{d}_{TS}) \ , \end{aligned} \tag{19}$$

where $\mathbf{R}_{\zeta}$, $\mathbf{R}_{uv}$, and $\mathbf{R}_{TS}$ are the error covariances of $\mathbf{e}_{\zeta}$, $\mathbf{e}_{uv}$, and $\mathbf{e}_{TS}$, respectively.

4. PRECONDITIONING OF COST FUNCTIONS

When all the matrices are given, the major computational task is to minimize the cost functions (17) using a minimization algorithm. When minimizing $J_c(\delta\mathbf{x}_c)$, defined by (17), a well-known numerical difficulty may be encountered in handling large-dimensional $\mathbf{B}_{\zeta'}$, $\mathbf{B}_{\psi''}$ and $\mathbf{B}_{TS}$ in J^{b}_{TS}, J^{b}_{ζ} and J^{b}_{uv}, which requires taking their inverse. In contrast, the observational cost functions J^{o}_{TS}, J^{o}_{ζ} and J^{o}_{uv} are generally less troublesome because $\mathbf{R}_{TS}$, $\mathbf{R}_{\zeta}$ and $\mathbf{R}_{uv}$ are mostly diagonal with nearly uniform values in the diagonal elements. These matrices are more like the identity matrix during the minimization procedure. The other primary numerical difficulty associated with minimization is that (17) might be ill-conditioned. When it is ill-conditioned, the minimization procedure may converge at a slow rate or not at all.[14] To improve the efficiency and reliability of the minimization procedure, preconditioning is often employed in 3DVAR (e.g., Courtier et al.[6]).

Here we introduce a particular preconditioning method. To formulate this method, we factorized the error covariance matrices as:

$$\begin{aligned} \mathbf{B}_{\zeta'} &= \mathbf{\Sigma}_{\zeta'}\mathbf{C}^{\xi\eta}_{\zeta'\zeta'}\mathbf{\Sigma}_{\zeta'} \\ \mathbf{B}_{\psi''\chi''} &= \mathbf{\Sigma}_{\psi''\chi''}\begin{pmatrix} \mathbf{C}^{\xi\eta\kappa}_{\psi''\psi''} & \mathbf{C}^{\xi\eta\kappa}_{\psi''\chi''} \\ \mathbf{C}^{\xi\eta\kappa}_{\chi''\psi''} & \mathbf{C}^{\xi\eta\kappa}_{\chi''\chi''} \end{pmatrix}\mathbf{\Sigma}_{\psi''\chi''} \\ \mathbf{B}_{TS} &= \mathbf{\Sigma}_{TS}\begin{pmatrix} \mathbf{C}^{\xi\eta\kappa}_{TT} & \mathbf{C}^{\xi\eta\kappa}_{TS} \\ \mathbf{C}^{\xi\eta\kappa}_{ST} & \mathbf{C}^{\xi\eta\kappa}_{SS} \end{pmatrix}\mathbf{\Sigma}_{TS} \ . \end{aligned} \tag{20}$$

Here $\mathbf{\Sigma}_{\zeta'}$, $\mathbf{\Sigma}_{\psi''\chi''}$, and $\mathbf{\Sigma}_{TS}$, are standard deviation matrices that are diagonal with the effective dimension being the same as the corresponding incremental vectors. Therefore, they can be used without simplification. Because of the assumption made for the errors among the five variable, there are five self correlation matrices, $\mathbf{C}^{\xi\eta}_{\zeta'\zeta'}$, $\mathbf{C}^{\xi\eta\kappa}_{\psi''\psi''}$, $\mathbf{C}^{\xi\eta\kappa}_{\chi''\chi''}$, $\mathbf{C}^{\xi\eta\kappa}_{TT}$, and $\mathbf{C}^{\xi\eta\kappa}_{SS}$, and two cross correlation matrices, $\mathbf{C}^{\xi\eta\kappa}_{\psi''\chi''} = (\mathbf{C}^{\xi\eta\kappa}_{\chi''\psi''})^T$ and $\mathbf{C}^{\xi\eta\kappa}_{TS} = (\mathbf{C}^{\xi\eta\kappa}_{ST})^T$. The superscripts of the correlation matrices indicate the spatial dimensionality of the correlation matrices, with ξ, η and κ for the cross-shore, alongshore, and vertical directions, respectively. The subscripts represent the two corresponding control variables. The cross correlation matrices $\mathbf{C}^{\xi\eta\kappa}_{\psi''\chi''}$ and $\mathbf{C}^{\xi\eta\kappa}_{TS}$ should not be confused with the correlation matrices of $\mathbf{C}_{\psi''\chi''}$ and $\mathbf{C}_{TS}$, that is,

$$\begin{aligned} \mathbf{C}_{\psi''\chi''} &= \begin{pmatrix} \mathbf{C}^{\xi\eta\kappa}_{\psi''\psi''} & \mathbf{C}^{\xi\eta\kappa}_{\psi''\chi''} \\ \mathbf{C}^{\xi\eta\kappa}_{\chi''\psi''} & \mathbf{C}^{\xi\eta\kappa}_{\chi''\chi''} \end{pmatrix} \\ \mathbf{C}_{TS} &= \begin{pmatrix} \mathbf{C}^{\xi\eta\kappa}_{TT} & \mathbf{C}^{\xi\eta\kappa}_{TS} \\ \mathbf{C}^{\xi\eta\kappa}_{ST} & \mathbf{C}^{\xi\eta\kappa}_{SS} \end{pmatrix} \ . \end{aligned} \tag{21}$$

We introduce preconditioning matrices, $\tilde{\mathbf{C}}_{\zeta'\zeta'}$, $\tilde{\mathbf{C}}_{\psi''\chi''}$ and $\tilde{\mathbf{C}}_{TS}$. They correspond to $\mathbf{C}^{\xi\eta}_{\zeta'\zeta'}$, $\mathbf{C}_{\psi''\chi''}$ and $\mathbf{C}_{TS}$, respectively. These three preconditioning matrices must: first, be symmetric and positive-definite; second, have the property that $\tilde{\mathbf{C}}^{-1}_{\zeta'\zeta'}\mathbf{C}_{\zeta'\zeta'} \approx I_{N_\zeta}$, $\tilde{\mathbf{C}}^{-1}_{\psi''\chi''}\mathbf{C}_{\psi''\chi''} \approx I_{N_{\psi\chi}}$ and $\tilde{\mathbf{C}}^{-1}_{TS}\mathbf{C}_{TS} \approx I_{N_{TS}}$, where I_{N_ζ}, $I_{N_{\psi\chi}}$ and $I_{N_{TS}}$ are identity matrices; and third, be easy to calculate their inversion and perform the Cholesky factorization, that is,

$$\begin{aligned}
\tilde{\mathbf{C}}_{\zeta'\zeta'} &= \tilde{\mathbf{L}}_{\zeta'\zeta'}\tilde{\mathbf{L}}^T_{\zeta'\zeta'}, && (22)\\
\tilde{\mathbf{C}}_{\psi''\chi''} &= \tilde{\mathbf{L}}_{\psi''\chi''}\tilde{\mathbf{L}}^T_{\psi''\chi''}, && (23)\\
\tilde{\mathbf{C}}_{TS} &= \tilde{\mathbf{L}}_{TS}\tilde{\mathbf{L}}^T_{TS}, && (24)
\end{aligned}$$

where $\tilde{\mathbf{L}}_{\zeta'\zeta'}$, $\tilde{\mathbf{L}}_{\psi''\chi''}$ and $\tilde{\mathbf{L}}_{TS}$ are lower triangular matrices and are referred to as Cholesky triangles.

With the Cholesky factorizations of $\tilde{\mathbf{C}}_{\zeta'\zeta'}$, $\tilde{\mathbf{C}}_{\psi''\chi''}$ and $\tilde{\mathbf{C}}_{TS}$ as in (24), we implement the transformation from $\delta\mathbf{x}_c$ to $\delta\mathbf{z}_c = (\delta\mathbf{z}^T_{\zeta'}, \delta\mathbf{z}^T_{\psi''\chi''}, \delta\mathbf{z}^T_{TS})^T$, defined by

$$\begin{aligned}
\delta\mathbf{x}_{\zeta'} &= \mathbf{\Sigma}_{\zeta'}\mathbf{C}_{\zeta'\zeta'}(\tilde{\mathbf{L}}^{-1}_{\zeta'})^T\delta\mathbf{z}_{\zeta'}\\
\delta\mathbf{x}_{\psi''\chi''} &= \mathbf{\Sigma}_{\psi''\chi''}\mathbf{C}_{\psi''\chi''}(\tilde{\mathbf{L}}^{-1}_{\psi''\chi''})^T\delta\mathbf{z}_{\psi''\chi''}\\
\delta\mathbf{x}_{TS} &= \mathbf{\Sigma}_{TS}\mathbf{C}_{TS}(\tilde{\mathbf{L}}^{-1}_{TS})^T\delta\mathbf{z}_{TS}\ . && (25)
\end{aligned}$$

This yields (17), the cost function of present ROMS3DVAR with $\delta\mathbf{z}_c$ as the control variables

$$\begin{aligned}
J_c(\delta\mathbf{z}_c) &= J^{\mathrm{b}}_{\zeta'}(\delta\mathbf{z}_{\zeta'}) + J^{\mathrm{b}}_{\psi''\chi''}(\delta\mathbf{z}_{\psi''\chi''}) + J^{\mathrm{b}}_{TS}(\delta\mathbf{z}_{TS})\\
&+ J^{\mathrm{o}}_{\zeta}(\delta\mathbf{z}_{\zeta'}, \delta\mathbf{z}_{TS}) + J^{\mathrm{o}}_{uv}(\delta\mathbf{z}_{\zeta'}, \delta\mathbf{z}_{\psi''\chi''}, \delta\mathbf{z}_{TS}) + J^{\mathrm{o}}_{TS}(\delta\mathbf{z}_{TS})\ , && (26)
\end{aligned}$$

where

$$\begin{aligned}
J^{\mathrm{b}}_{\zeta'} &= \frac{1}{2}\delta\mathbf{z}^T_{\zeta'}\tilde{\mathbf{L}}^{-1}_{\zeta'}\mathbf{C}_{\zeta'\zeta'}(\tilde{\mathbf{L}}^{-1}_{\zeta'})^T\delta\mathbf{z}_{\zeta'},\\
J^{\mathrm{b}}_{\psi''\chi''} &= \frac{1}{2}\delta\mathbf{z}^T_{\psi''\chi''}\tilde{\mathbf{L}}^{-1}_{\psi''\chi''}\mathbf{C}_{\psi''\chi''}(\tilde{\mathbf{L}}^{-1}_{\psi''\chi''})^T\delta\mathbf{z}_{\psi''\chi''},\\
J^{\mathrm{b}}_{TS} &= \frac{1}{2}\delta\mathbf{z}^T_{TS}\tilde{\mathbf{L}}^{-1}_{TS}\mathbf{C}_{TS}(\tilde{\mathbf{L}}^{-1}_{TS})^T\delta\mathbf{z}_{TS}, && (27)
\end{aligned}$$

are the preconditioned background cost function (18).

$$\begin{aligned}
J^{\mathrm{o}}_{\zeta'} &= \frac{1}{2}(\mathbf{H}_\zeta\delta\mathbf{x}^\dagger_\zeta - \mathbf{d}_\zeta)^T\mathbf{R}^{-1}_\zeta(\mathbf{H}_\zeta\delta\mathbf{x}^\dagger_\zeta - \mathbf{d}_\zeta)\\
J^{\mathrm{o}}_{uv} &= \frac{1}{2}(\mathbf{H}_{uv}\delta\mathbf{x}^\dagger_{uv} - \mathbf{d}_{uv})^T\mathbf{R}^{-1}_{uv}(\mathbf{H}_{uv}\delta\mathbf{x}^\dagger_{uv} - \mathbf{d}_{uv})\\
J^{\mathrm{o}}_{TS} &= \frac{1}{2}(\mathbf{H}_{uv}\delta\mathbf{x}^\dagger_{TS} - \mathbf{d}_{TS})^T\mathbf{R}^{-1}_{TS}(\mathbf{H}_{uv}\delta\mathbf{x}^\dagger_{TS} - \mathbf{d}_{TS}) && (28)
\end{aligned}$$

are observational cost functions (19) that are not preconditioned with respect to $\delta\mathbf{z}_c$. Here

$$\begin{aligned}
\delta\mathbf{x}^\dagger_\zeta &= \mathbf{\Sigma}_{\zeta'}\mathbf{C}_{\zeta'\zeta'}(\tilde{\mathbf{L}}^{-1}_{\zeta'})^T\delta\mathbf{z}_{\zeta'} + \mathbf{\Pi}_{TS}\mathbf{\Sigma}_{TS}\mathbf{C}_{TS}(\tilde{\mathbf{L}}^{-1}_{TS})^T\delta\mathbf{z}_{TS}\\
\delta\mathbf{x}^\dagger_{uv} &= \mathbf{\Gamma}_{\zeta'}\mathbf{\Sigma}_{\zeta'}\mathbf{C}_{\zeta'\zeta'}(\tilde{\mathbf{L}}^{-1}_{\zeta'})^T\delta\mathbf{z}_{\zeta'} + \mathbf{\Gamma}_{TS}\mathbf{\Sigma}_{TS}\mathbf{C}_{TS}(\tilde{\mathbf{L}}^{-1}_{TS})^T\delta\mathbf{z}_{TS} + \mathbf{\Phi}\mathbf{\Sigma}_{\psi''\chi''}\mathbf{C}_{\psi''\chi''}(\tilde{\mathbf{L}}^{-1}_{\psi''\chi''})^T\delta\mathbf{z}_{\psi''\chi''}\\
\delta\mathbf{x}^\dagger_{TS} &= \mathbf{\Sigma}_{TS}\mathbf{C}_{TS}(\tilde{\mathbf{L}}^{-1}_{TS})^T\delta\mathbf{z}_{TS} && (29)
\end{aligned}$$

correspond to the increment $\delta\mathbf{x}$ in the full model space (5) but are computed from $\delta\mathbf{z}_c$ using preconditioning (25) as well as the dynamical constraints (12) and (13).

The preconditioned cost function (26) offers two important merits. $J^{\mathrm{b}}_{\zeta'}$, $J^{\mathrm{b}}_{\psi''\chi''}$ and J^{b}_{TS} are well conditioned; and the inversion of the error correlation matrices is no longer necessary in any of the J^b.

5. CONSTRUCTION OF PRECONDITIONING CORRELATION MATRICES

5.0.1 Approach

For convenience, we introduce some new notation. Since ROMS employs curvilinear linear coordinates, we assume that the horizontal coordinates are in the cross-shore and alongshore directions. For simplicity, we consider a model grid box of dimensions $N^\xi \times N^\eta \times N^\kappa$. Extension to an irregular model grid is straightforward.

Since the same formulation is used for the construction of all five self-correlation matrices, we simply use the notation $\mathbf{C}$ in the following discussion. We further employ the following notations: $\mathbf{C}^\xi$ for any one-dimensional (1D) cross-shore correlation matrix with dimension $(N^\xi)^2$; $\mathbf{C}^\eta$ for any 1D alongshore correlation matrix with dimension $(N^\eta)^2$; $\mathbf{C}^{\xi\eta}$ for any two-dimensional (2D) horizontal correlation matrix with dimension $(N^\xi N^\eta)^2$ and $\mathbf{C}^{\xi\kappa}$ for any 2D vertical cross-shore correlation matrix with dimension $(N^\xi N^\kappa)^2$ and $\mathbf{C}^{\xi\eta\kappa}$ for any three-dimensional (3D) correlation matrix with the dimension $(N^\xi N^\eta N^\kappa)^2$. Generally 1D correlations are manageable, and can be constructed with various methods, while simplification is necessary for the 2D and 3D correlations for a sophisticated model. As correlation matrices, any $\mathbf{C}$ must be positive definite.

The formulation of constructing correlations proposed here hinges on the Kronecker product. The Kronecker product is also known as the tensor product or direct product. For its general definition and properties, readers are referred to Graham.[15]

5.0.2 Two-Dimensional Error Correlation $\mathbf{C}^{\xi\eta}$

With the Kronecker product we construct a 2D correlation matrix $\mathbf{C}^{\xi\eta}$ from two 1D correlation matrices, $\mathbf{C}^\xi$ and $\mathbf{C}^\eta$:

$$\mathbf{C}^{\xi\eta} = \mathbf{C}^\eta \otimes \mathbf{C}^\xi. \tag{30}$$

This is practically equivalent to choosing writing the elements of $\mathbf{C}^{\xi\eta}$ to be the correlations between the 2D grid points $(i_1 : j_1)$ and $(i_2 : j_2)$ given by

$$C^{\xi\eta}(i_1 : j_1, i_2 : j_2) \;=\; C^\xi(i_1, i_2)\; C^\eta(j_1, j_2), \tag{31}$$

where $C^\xi(i_1, i_2)$ is the element of $\mathbf{C}^\xi$ corresponding to correlation between the 1D ξ-grid points i_1 and i_2, and $C^\eta(j_1, j_2)$ follows the same convention for 1D η-grid points. Quantitatively, such a $\mathbf{C}^{\xi\eta}$ can be an accurate approximation to the 2D correlation in many circumstances.

One desirable characteristic of the Kronecker product formulation is that we can directly construct relatively sophisticated 2D anisotropic and inhomogeneous correlations using data. With the NMC method, we can construct the 2D correlations as follows. The element of the 1D correlation $\mathbf{C}^\xi$ is computed as the correlation between the two columns of the model grids, and the element of the 1D correlation $\mathbf{C}^\eta$ as the correlation between two rows of the model grids. The 2D correlation can then be constructed with the Kronecker product of $\mathbf{C}^\xi$ and $\mathbf{C}^\eta$.

5.0.3 Three-Dimensional Error Correlation $\mathbf{C}^{\xi\eta\kappa}$

Like horizontal 2D error correlation matrices, a 3D error correlation matrix can also be constructed using the Kronecker product formulation. In a simple form it may be constructed from the three 1D correlation matrices $\mathbf{C}^\xi$, $\mathbf{C}^\eta$, and $\mathbf{C}^\kappa$, that is, $\mathbf{C}^{\xi\eta\kappa} = \mathbf{C}^\xi \otimes \mathbf{C}^\eta \otimes \mathbf{C}^\kappa$, where $\mathbf{C}^\kappa$ is the 1D correlation matrix in the vertical direction. This formulation implies the separability of the correlations in the three spatial dimensions. For coastal oceans, horizontal separability may be acceptable. Also, the separability between the alongshore and vertical directions can be used when the model domain does not span a long distance alongshore, and when the coastline is relatively straight such as the area off California. However, the correlation is usually not separable between the vertical and cross-shore directions, because the vertical correlation function depends on the distance away from the coastline cross-shore. This dependence can be significant especially when strong upwelling is present. The upwelling raises the thermocline nearshore, and results in a shallower mixing layer nearshore than in the areas farther off shore. The difference in the mixing layer vertical structure, in turn, causes the difference in the vertical correlation.

Such inseparability of the correlation between the vertical and cross-shore directions can be incorporated using the Kronecker product formulation. To do so, we first construct the 2D error correlation $\mathbf{C}^{\xi\kappa}$. The 3D correlation is then constructed with the Kronecker product

$$\mathbf{C}^{\xi\eta\kappa} = \mathbf{C}^{\xi\kappa} \otimes \mathbf{C}^\eta. \tag{32}$$

5.0.4 Computational Issues

Having described the construction of the anisotropic, inhomogeneous and inseparable 3D error correlation $\mathbf{C}^{\xi\eta\kappa}$ using the Kronecker product formulation, we now describe some computational issues in implementing $\mathbf{C}^{\xi\eta\kappa}$ in 3DVAR. The Kronecker product formulation requires limited memory. For a coastal ocean model the number of grid points in both the alongshore and cross-shore directions are on the order of $O(10^3)$, and the number of the vertical levels is on the order of $O(10^1)$. Therefore, the memory required to define a symmetric matrix $\mathbf{C}^{\xi\eta\kappa}$ is $\frac{1}{2}(N^{\xi}N^{\kappa})^2 + \frac{1}{2}(N^{\eta})^2$ and is of $O(10^8)$. This memory requirement is easily satisfied by present day computers. Further, the positive definiteness of $\mathbf{C}^{\xi\eta\kappa}$ is guaranteed if $\mathbf{C}^{\xi\kappa}$ and $\mathbf{C}^{\eta}$ are individually positive definite.

6. EVALUATION OF FORECASTS

Construction of error covariances is central to the development of any 3DVAR system. The performance of ROMS3DVAR hinges on the accurate description of $\mathbf{B}$ and $\mathbf{R}$ in (18) and (19). Here $\mathbf{B}$ is considered to be identical to the preconditioning matrices, while $\mathbf{R}$ are considered a diagonal matrix.

ROMS has a one-way nesting capability. A three-level, nested configuration is used in this study: the largest level (L0) covers the U.S. West Coastal Ocean at the horizontal resolution 15km; the next level (L1) is nested in L0 over the central California coastal ocean at the horizontal resolution of 5km; the last level (L2) is nested in L1 and focuses on the region around Monterey Bay at the horizontal resolution of 1.5km All three nested levels have 32 layers in the vertical. In the discussion below, we focus on L2 only. Figure 1 shows the bathymetry and horizontal model domain of L2, which is surrounded by the California coast on the eastern side and open ocean on the other three sides. A prominent feature of the bathymetry is the narrow shelf whose width varies along the coast. The slope is particularly steep along the Monterey Submarine Canyon. The numerical algorithms of ROMS are specifically designed to reduce pressure gradient errors associated with steep topography.[2]

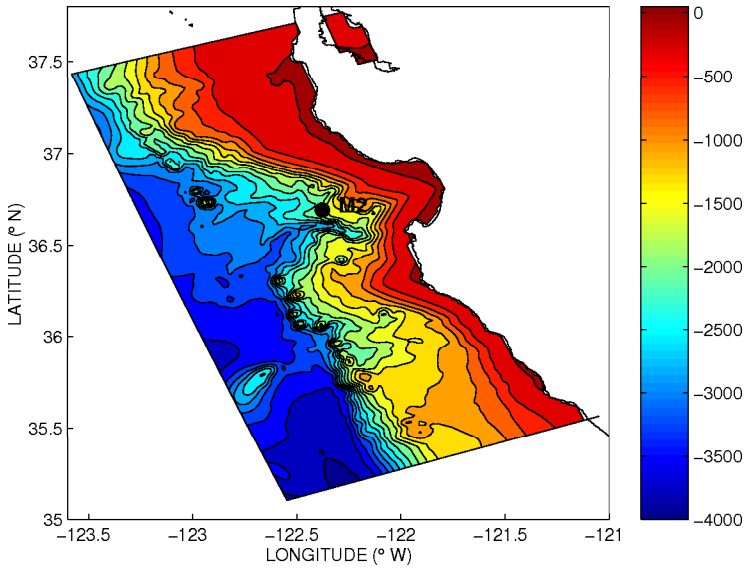

Figure 1. The L2 domain and bathymetry. The bathymetry contour interval is 250m. The black circle shows the location of M2 mooring at 122.378°W and 36.697°N. The sharp trough near M2 is the Monterey Submarine Canyon.

The AOSN experiment in Monterey Bay, California, August 2003, provided an unprecedented number of *in situ* observations by a variety of means and instruments; details of the experiment can be found at the WWW site (http://www.mbari.org/aosn). During August 2003, ROMS3DVAR generated analyses and forecasts in real-time using the 6h forecast cycle. After the experiment, additional observations became available while some of the original observations were upgraded. The results presented in this section are obtained using all observations available. The observations include the NAVOCEANO MCSST Level 2 High Resolution Picture Transmission and Local Area Coverage (HRPT/LAC) 2.2km sea surface temperature dataset (Level 2),

HFradar sea surface velocity measurements, underwater glider temperature/salinity profiles, aircraft SSTs, ship temperature/salinity/depth (CTD), and Automatic Underwater Vehicle (AUV) temperature/salinity profiles (http://www.mbari.org/aosn for details about observations).

6.0.5 An Analysis of T/S Profiles

Here we present an analysis on 24h forecast by using M2 observations. Figure 2 shows the comparison between the 24h forecast and M2 observations. The difference between the observations and 24h forecasts (2nd row), which is known as forecast errors, shows a maximum of about 2°C in temperature and 0.25psu in salinity. To illustrate the implication of such forecast errors, we compare the forecast errors with the 24h changes in the M2 observations (bottom row). The maximum of 24h changes of the M2 observations is as large as 4°C in temperature and 0.3psu in salinity. While the forecast error is significant in comparison with the 24h changes, the forecast error is smaller than the 24h change.

By further examination, we can see that the 24h change of the M2 observation shows three significant transitions associated with the upwelling and relaxation events. The temperature decreases and the salinity increases between Aug. 5 and Aug. 15 in association with the development of the upwelling event. During the late stage of the upwelling event between Aug. 15 and Aug 19, the temperature increases and salinity decreases. The strongest change occurs during the relaxation between Aug. 19 and Aug. 22; the temperature decreases as much as 4°C and salinity increases as much as 0.3psu. The skill of the 24h forecasts depends on the ability of the model to predict these transitions. As such, we analyze the forecast 24h change (3rd row), which is defined as the difference between the 24h forecast and its corresponding initial condition, i.e., the analysis. The similarity between the forecast and observation 24h change shows a non-trivial 24h forecast skill.

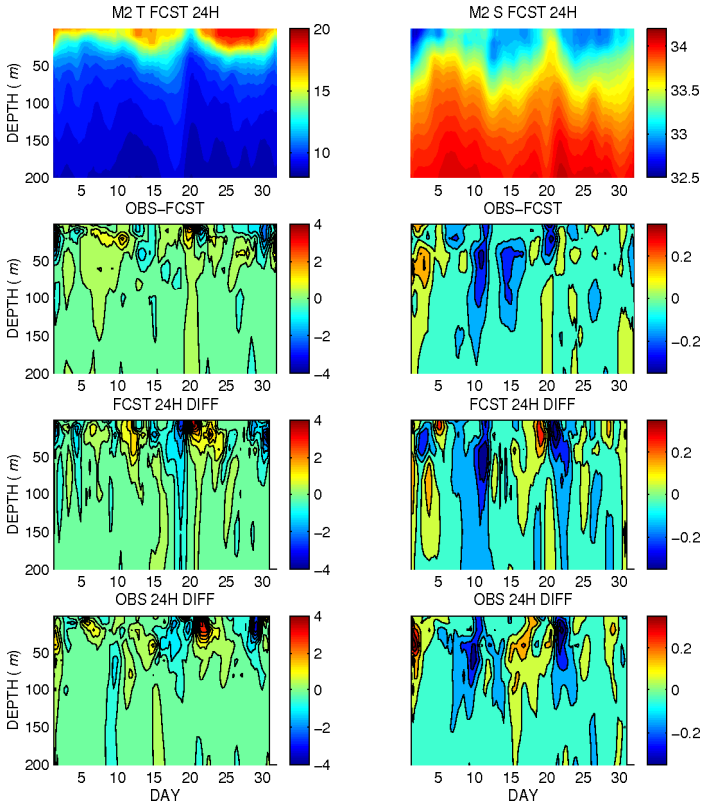

Figure 2. Comparison of the 24h forecast and the M2 observation for August 2003. The left column is temperature, and the right column is salinity. The temporal evolution of the 24h forecasts are shown in the top row; the difference between the M2 observations and 24h forecast in the second row; the 24h forecast change (i.e., 24h forecasts minus the corresponding analyses used as initial conditions) in the third row; and the 24h change of M2 observations in the bottom row. The contour interval is 0.5°C for temperature and 0.1psu for salinity.

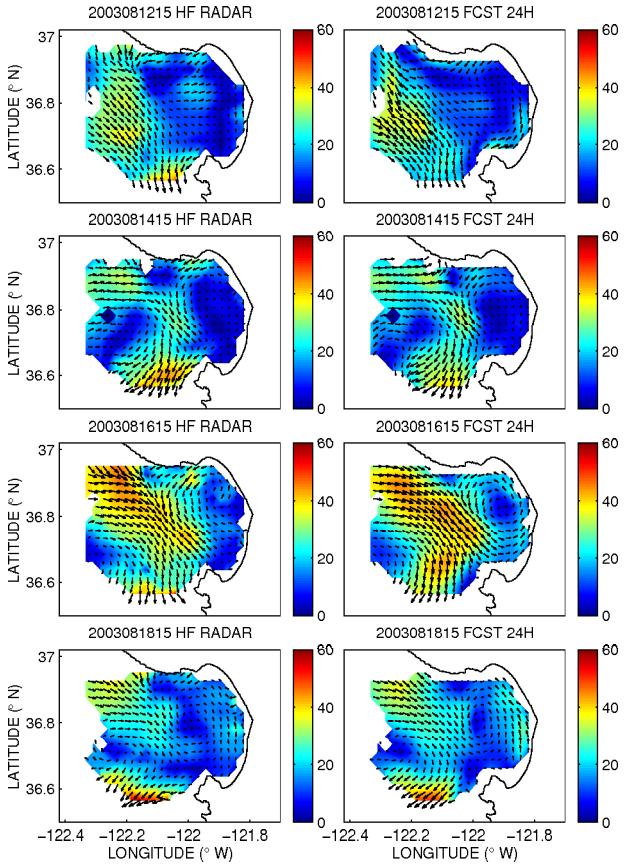

Figure 3. The HF radar sea surface current measurements and 24h forecasts during the upwelling Event that occurred during the Autonomous Ocean Sampling Network experiment between August 10-19, 2003.

6.0.6 Surface Velocity by the High-Frequency Radar

The HF radar covers mainly Monterey Bay where ageostrophic component is significant. Moreover, the tidal velocity in this region can be as large as $0.1 - 0.2$m/s, which is comparable to the velocity arising from dynamic processes. The forecast of currents near Monterey Bay is a challenge.

During the upwelling period the HF radar observation shows the formation of a jet-like structure that swerves in and out of the bay with a high speed. It also shows the formation of a cyclonic circulation within the bay. They are reproduced in the 24h forecast as shown in Fig.3.

To quantify the agreement of ROMS3DVAR with the observation, we use the correlation of the flow pattern between the HF radar observation and the ROMS3DVAR forecast. The correlation is defined by

$$corr = \frac{\Sigma_{m=1}^{M^{HF}}[(u_m^{HF} - \overline{u}^{HF})(u_m^{\mathrm{a}} - \overline{u}^{\mathrm{a}}) + (v_m^{HF} - \overline{v}^{HF})(v_m^{\mathrm{a}} - \overline{v}^{\mathrm{a}})]}{\sqrt{\Sigma_{m=1}^{M^{HF}}[(u_m^{HF} - \overline{u}^{HF})^2 + (v_m^{HF} - \overline{v}^{HF})^2]}\sqrt{(\Sigma_{m=1}^{M^{HF}}[(u_m^{\mathrm{a}} - \overline{u}^{\mathrm{a}}) + (v_m^{\mathrm{a}} - \overline{v}^{\mathrm{a}})^2]}} \,. \tag{33}$$

M^{HF} is the number of the HF radar observation for the corresponding event, the superscript HF stands for the HF radar, and $\overline{\{\cdot\}}$ for the average over M^{HF} observation. The average correlation is as high as 0.78 during the upwelling.

7. SUMMARY

A 3DVAR data assimilation scheme, called ROMS3DVAR, has been developed in support of Coastal Ocean Observing Systems. ROMS is employed as the oceanic forecast model. In recognition of the dynamic complexities of

coastal oceans, we comprehensively and carefully incorporated dynamic balance constraints, constructed forecast error covariances, and preconditioned the cost function.

The dynamic constraints are incorporated to keep the analysis in the desirable dynamic balance. In ROMS3DVAR, weak dynamic constraints are formulated in the framework of the maximum-likelihood estimation.[16] It follows the method of partitioning for the balanced and unbalanced parts.[9] Applying the partition to the increments, rather than the total field, ROMS3DVAR maintains the internal dynamic consistency with the forecast $\mathbf{x}^{\mathrm{f}}$, which can be subtle and delicate in a coastal ocean model.

The dynamic constraints are incorporated not only for keeping the analysis near the dynamic balance, but also for improving the cross correlations between the control variables. The cross correlations between velocity components and T/S are mainly the consequence of geostrophic and hydrostatic balance. In ROMS3DVAR the incremental steric SSH and geostrophic velocity components are determined by the incremental temperature and salinity. The control variables are then transformed into incremental non-steric SSH, ageostrophic streamfunction and velocity potential, temperature and salinity. In this way the cross-correlations among non-steric SSH, ageostrophic streamfunction and velocity potential, and temperature and salinity are neglected in ROMS3DVAR.

A Kronecker product formulation has been proposed to construct forecast error correlations. The most important capability of this formulation is its ability to represent 3D inhomogeneous and anisotropic correlations. The inhomogeneity and anisotropy in the forecast error covariance are significant and ubiquitous in coastal oceans. The significance and ubiquity is due to the control of the dynamics of coastal oceans by two primary physical boundaries: the sea surface and the coastline. The atmosphere drives the ocean at its surface; therefore, more dramatic changes in the ocean occur near the surface than in the deep water. The difference is dramatically manifested by the existence of the thermocline. Such a vertical difference in the dynamics necessarily leads to a vertical difference in forecast error correlations. For the horizontal correlations, they are influenced by the coastline. The structure of the forecast error correlation is thus a function of the distance from the coastline. The Kronecker product formulation has the capability of modeling such inhomogeneity and anisotropy.

The Kronecker product formulation also offers computational advantages. One advantage is the limited memory requirement for the error correlation. The memory required is manageable on present day supercomputers for typical coastal ocean models. The most important computational advantage of the Kronecker product formulation is that the Cholesky factorizations of the 3D correlation matrices can be implemented directly.

The experiment with the AOSN observations demonstrated the capability of reproducing complex flow patterns during upwelling and relaxation, as well as the transition between the upwelling and relaxation regimes. It is especially encouraging that the result from ROMS3DVAR showed useful skills for 24h forecasts in comparison with the mooring observations and the HF radar surface velocity observations. Note that the mooring is located in the Monterey Submarine Canyon, while the HF radar measures the area over the Canyon head. These locations always present great challenges to coastal ocean modelers. The success of the data assimilation in these locations indicates that ROMS3DVAR has the capability of coping with complex bathymetry and dynamics.

ACKNOWLEDGMENTS

The research described in this publication was carried out, in part, the Jet Propulsion Laboratory (JPL), California Institute of Technology, under a contract with the National Aeronautics and Space Administration (NASA). Computations were performed on the SGI Origin computer through the JPL Supercomputing Project. Support from the Office of Naval Research (ONR) under the grant numbers N00014-04-1-0166, N00014-04-1-0191, N00014-04-1-0401 and N00014-05-1-0293 is gratefully acknowledged.

REFERENCES

1. E. Kalnay, *Atmospheric modeling, data assimilation and predictability*, Cambridge Univ. Press, New York, 2003.
2. A. F. Shchepetkin and J. C. McWilliams, "The regional ocean modeling system: A split-explicit, free-surface, topography-following-coordinateocean model," *Ocean modeling* **9**, pp. 347–404, 2005.
3. P. Marchesiello, J. C. McWilliams, and A. F. Shchepetkin, "Open boundary conditions for long-term integration of regional ocean models," *Ocean Modelling* **3**, pp. 1–20, 2001.

4. J. Paduan and H. C. Graber, "Introduction to high-frequency radar: Reality and myth," *Oceanography* **10**, pp. 36–39, 1997.
5. K. Ide, P. Courtier, M. Ghil, and A. Lorenc, "Unified notation for data assimilation: Operational sequential and variational," *J. Meteor. Soc. Japan* **75, 1B**, pp. 71–79, 1997.
6. P. Courtier, J. Thepaut, and A. Hollingsworth, "A strategy for operational implementation of 4d-var, using an incremental approach," *Quart. J. Roy. Meteorol. Soc.* **120**, pp. 1367–1388, 1994.
7. J. McWilliams, N. J. Norton, P. R. Gent, and D. B. Haidvogel, "A linear balance model of wind-driven, mid-latitude ocean circulation," *J. Phys. Oceanogr.* **20**, pp. 1349–1387, 1990.
8. Z. Li, Y. Chao, J. C. McWilliams, and K. Ide, "A three-dimensional variational data assimilation scheme for the regional ocean modeling system: Implementation and basic experiments," *J. Geophy. Res.* **Submitted**, 2007.
9. D. F. Parrish and J. C. Derber, "The national meteorological center's spectral-interpolation system," *Mon. Weather Rev.* **120**, pp. 1747–1763, 1992.
10. A. C. Lorenc, "Modelling of error covariances by 4d-var data assimilation," *Quart. J. Roy. Meteorol. Soc.* **129**, pp. 2991–3012, 2003.
11. D. M. Barker, W. Huang, Y. Guo, A. Bourgeois, and Q. N. Xiao, "A three-dimensional variational data assimilation system for mm5: Implementation and initial results," *Mon. Weather. Rev.* **132**, pp. 897–914, 2004.
12. R. Daley, *Atmospheric Data Assimilation, Cambridgeatmospheric and space science series*, Cambridge University Press, Cambridge, UK, 1991.
13. Z. Li, Y. Chao, and J. C. McWilliams, "Computation of the streamfunction and velocity potential for limited and irregular domains," *Mon. Weather Rev.* **134**, pp. 3384–3304, 2006.
14. J. Nocedal and S. J. Wright, *Numerical Optimization*, Springer-Verlag, New York, 1999.
15. A. Graham, *Kronecker product and matrix Calculus with Applications*, Ellis Horwood Ltd., Chichester, England, 1981.
16. A. H. Jazwinski, *Stochastic processes and filtering theory*, Academic Press, New York, 1970.